Published in final edited form as:
Circ J. 2010 October ; 74(10): 2079–2088.

Synergistic Dual Automaticity in Sinoatrial Node Cell and Tissue Models

Hong Zhang, PhD[1,2], **Boyoung Joung, MD, PhD**[3], **Tetsuji Shinohara, MD, PhD**[1], **Mei Xi, MD**[2], **Peng-Sheng Chen, MD**[1], and **Shien-Fong Lin, PhD**[1]

[1] Krannert Institute of Cardiology and the Division of Cardiology, Department of Medicine, Indiana University School of Medicine, Indianapolis, Indiana, USA

[2] School of Electrical Engineering, Xi'an Jiaotong University, Xi'an, Shaanxi, China

[3] Yonsei Cardiovascular Center and Cardiovascular Research, Yonsei University, Seoul, Korea

Abstract

Background—The mechanism of sinoatrial node (SAN) automaticity is traditionally attributed to membrane ion currents. Recent evidence indicates spontaneous sarcoplasmic reticulum (SR) Ca^{2+} cycling also plays an important role.

Methods and Results—We performed computer simulation on SAN cell and 1D tissue model. In the SAN cells, SR Ca^{2+} cycling broadly modulated sinus rate from 1.74Hz to 3.87Hz. Shortening of the junctional SR refilling time and increase of SR Ca^{2+} release were responsible for sinus rate acceleration. However, under the fast SR Ca^{2+} cycling, decreased L-type Ca^{2+} current (I_{CaL}) resulted in irregular firing. When Ca^{2+} cycling was suppressed, I_f and I_{CaT} both acted to stabilize the pacemaker rhythm, but I_{CaT} had less effect than I_f. At the 1D level, the electrical coupling between neighboring cells had little effect on the earliest pacemaker location. The leading pacemaking site always colocalized with the site with the highest SR Ca^{2+} cycling rate, but shifted to the site with less inhibited I_{CaL}.

Conclusions—The rate of SR Ca^{2+} cycling can effectively and broadly modulate the sinus rate. I_f, I_{CaL} and I_{CaT} play integral roles to guarantee SAN cell rhythmic firing. The leading pacemaker site is determined by intracellular Ca^{2+} dynamics and membrane currents, indicating the synergistic dual automaticity not only exists in single SAN cells, but also at the tissue level.

Introduction

The sinoatrial node cells (SANC) are the primary pacemakers of the heart. They spontaneously exhibit slow diastolic depolarization (DD) to a threshold for firing, thereby periodically initiating action potentials to set the rhythm of the heart[1, 2]. Spontaneous DD has traditionally been attributed to a "membrane clock (M clock)" mechanism [3, 4], in which the membrane potential changes with the activation and inactivation of the membrane ion channel currents. Recently, the "Ca^{2+} clock" has been put forward as a complementary mechanism for SAN automaticity[5, 6]. Results from single SANC studies suggested that isolated sarcoplasmic reticulum (SR) could operate as a self-sustained Ca^{2+} oscillator and a small spontaneous Ca^{2+} release from the junctional SR to the intracellular subspace occurred first as the initiating event, which in turn activated Na^+/Ca^{2+} exchanger current (I_{NCX}) and caused the accelerated DD. With these experimental results, a mathematical model of SANC was recently constructed

Corresponding Author: Shien-Fong Lin, PhD, 1801 N. Capitol Ave, E 308, Indianapolis, IN 46202., Phone : 317-962-0121: linsf@iupui.edu.

to include the intracellular Ca^{2+} cycling together with the more traditional ionic channel currents [7]. On the other hand, at the tissue level, the functional organization of SANC is still not very clear today. This makes evaluation of the interaction between the two clocks especially challenging.

The synergistic action of the M and Ca^{2+} clocks has been demonstrated by the Maltsev-Lakatta model[7], but previous works did not extensively explore mechanisms of heart rate modulation. Furthermore, it is unclear whether the two clock synergy can be applied to multicelluar SAN structures to determine the dominant pacemaking site. In this paper, by introducing a variety of simulated interventions, such as β-adrenergic stimulation, I_{CaL} and I_{CaT} alteration, on a single cell and a constructed tissue model, we evaluated the synergistic effects of two clocks on the rhythmic firing and leading pacemaker site.

Method

The single cell model and its solution

We selected the Maltsev-Lakatta SAN rabbit model [7] for the current study because it is the latest and most advanced numerical formulations to address dynamic activities of the SR Ca^{2+} pump and ion buffering in all cell compartments, including Ca^{2+} buffering by calsequestrin in junctional SR (jSR). The model included twenty nine first-order differential equations with the following format to describe action potential of a single SANC:

$$\frac{dV}{dt} = -\frac{1}{C_m}(I_{ion}) \tag{1}$$

where V was the transmembrane potential, C_m was the membrane capacitance, t was the time, I_{ion} was the total ionic current.

In general I_{ion} was a function of the voltage V and gating variables $Y_1,\ldots Y_i,\ldots Y_M$ that satisfied the following ordinary differential equations:

$$\begin{gathered}\frac{dY_i}{dt} = \frac{I_{i\_\inf} - Y_i}{\tau_{Y_i}} \quad i = 1, \ldots, \mathrm{M}, \\ Y_{i\_\inf} = \frac{\alpha_i}{\alpha_i + \beta_i} \\ \tau_{Y_i} = \frac{1}{\alpha_i + \beta_i}\end{gathered} \tag{2}$$

where Y_{i_inf} was the steady-state value of the gating variable Y_i. τ_{Yi} was its time constant. α_i, β_i were opening and closing rates of the channel gating.

Ca^{2+} release from the SR via ryanodine receptors (RyRs)[8], its intracellular fluxes, buffering, and concentrations in cell compartments satisfied another set of ordinary differential equations.

$$\frac{dZ_i}{dt} = f(j, r) \tag{3}$$

where Z_i, j, r were a variety of introduced variables, such as Ca^{2+} concentrations in different cell compartment or flux coefficients during dynamic processes.

The fourth-order Runge-Kutta method was applied to integrate the single cell model with a time step of 0.005ms. Decreasing the time step to 0.001ms was not found to change the simulation results.

One-dimensional SAN tissue and its numerical integration

Cardiac tissue could be treated as a continuous and excitable medium connected by gap junctions between adjacent cells. If only the intracellular space was taken into account, the tissue was considered as a monodomain system. Then Eq.4 could be used to describe the tissue, together with the no-flux boundary conditions imposed at both ends of the fiber as described by Eq.5.

$$C_m \frac{\partial V}{\partial t} = -(I_{ion}) + \frac{1}{\rho_x S_v} \frac{\partial^2 V}{\partial x^2} \tag{4}$$

$$(\nabla V)|_{x=0} = (\nabla V)|_{x=l} = 0, \tag{5}$$

where x was the spatial coordinates in the string of tissue, ρ_x was the bulk cytoplasmic resistivity, S_v was the surface-to-volume ratio, and l was the length of the whole fiber.

SAN central area is normally the dominant pacemaker location. To explore the role of SR Ca^{2+} dynamics in determining the leading pacemaker site, we performed simulation around the central SAN region. The fiber consisted of 30 cells with strand length of 0.3cm that was approximately half the length of SA node in the rabbit [9], and parallel to the direction of the superior to the inferior vena cava which was consistent with extension direction of the central SANC [10]. The fiber was divided into three parts: cells from the first to the 10^{th} were designated the inferior part, the 11^{th} to 20^{th} cells middle part, and the left 10 cells superior part.

So far, two models (mosaic and gradient model) of the organization of SAN tissue have been put forward[11]. According to the mosaic model, all SANC had reasonably uniform properties, it was the peppered atrial myocytes that made them show the different morphology. Recently, a mix of atrial and SAN cells in the SAN tissue periphery was reported, but no atrial cells were found in the SAN central area [10], indicating that our concerned region could be considered homogeneous in the controlled condition. In the gradient model[12], it was suggested that SANCs showed transition of electrophysiological properties from the center to the periphery. An empirical exponential formula was given to describe changes of parameters such as cellular size and current conductances. According to this formula, these parameters almost kept the same within half length of the fiber, and only started to show heterogeneity close to the defined periphery. This implied that the central region was also considered uniform in this organization. Therefore, based on these two models, our concerned region could be set homogeneous to the controlled condition.

It was reported that the leading pacemaker site changed dynamically within the central area because of interventions affecting different regions of the node differentially [13, 14, 15]. For β-adrenergic stimulation, there has been little report about heterogeneous sensitivities among primary pacemakers. Our main purpose here is to investigate relationship between the leading pacemaker site and SR Ca^{2+} activity, therefore the exact form of its distribution has less significance on the results. In this case, we hypothesized three kinds of heterogeneity: one was a linear change of SERCA pump rate(P_{up}) from the superior to the inferior parts along the fiber. The second adopted an exponential change from the putative equation 80 [12] shown in

formula (6). The third was a discontinuous state: the middle cells had higher P_{up} than the superior and inferior cells. On the basis of such a discontinuity, P_{up} in different parts of the SAN received different percentage of increase to investigate whether the leading pacemaker site shifted with P_{up}.

$$F_{cell}=1.07\times 29.0\times \frac{1.0\times(30-n)}{cell\_number}/(30.0\times(1.0+0.7745\times\exp(-(29.0\times\frac{1.0\times(30-n)}{cell\_number}-24.5)/1.95))) \quad (6)$$

where n stands for the numbered cell, *cell_number* is the total amount of cells in the tissue (here *cell_number* = 30), F_{cell} is a scaling factor of P_{up}, which is directly based on the location of a cell relative to the firstSAN.

Assuming that all cells were cylindrical and adhered to the dimensions suggested in the Maltsev-Lakatta's single cell model, a radius of 4.0 μm and length of 70μm were used for all cells in the fiber, resulting in a surface-to-volume ratio $S_v = 5300\text{cm}^{-1}$. According to the experimental data obtained in pairs of rabbit SANC using the double whole-cell patch clamp technique [16], the mean conductivity value of the intercellular coupling was 7.5nS. Therefore, based on the Eq.86 of [12] in which at each grid point the conductivity tensor was determined from both the intercellular conductivity and the dimensions of the cell, we used $\rho_x = 9.57 \times 10^{-6}$ GΩ ··cm at each grid point in our tissue simulation. The model was considered a monodomain and continuum system, thus the geometry of the cells and gap junctions would not significantly affect the results of computation.

The three-point centered difference method with spatial step of $\Delta x = h = 0.01$cm was used in the calculation. Source code was developed by us using C++ programming language and all simulations were performed on a personal computer.

Results

Intracellular SR Ca^{2+}cycling

Two main parameters, a SERCA pump rate P_{up} and a Ca^{2+} release rate K_s, were included in the model to account for the operation of the cardiac SR. In Ref.[7], by removing the membrane clock (all ion currents = 0), the investigators analyzed characteristics of the isolated SR Ca^{2+} in simultaneous P_{up} and K_s changes. We simulated their combined effects on sinus rate regulation with the intact two clocks (Fig. 1). Panel A showed that spontaneous action potential could be generated within a broad frequency ranging from 1.74Hz to 3.87Hz. Increasing P_{up} accelerated sinus rate whereas decreasing K_s had the opposite effect. Under slow sinus rate the diastolic depolarization was markedly prolonged with slight hump-like elevation during DD comparing (b) with (a)in Panel B. When either P_{up} or K_s was greatly reduced from their baseline values (P_{up} =12mM/s, *K*s =250/μs), irregular firing and intermittent sinus pause (Fig. 1Bc and Fig. 1Bd) occurred in the grey zone.

Fig. 2 displayed internal processes of sinus rate regulation by P_{up} and K_s. According to Ref. [7], Ca^{2+} release from the jSR was divided into three stages (Fig. 2G and green arrows in the inset on the right): the first spontaneous primary release (during mid-DD), a secondary larger release (during late DD indicated by the grey bars) and the third AP-induced release (Ca^{2+}-induced Ca^{2+} release or CICR[17] due to activation of L-type Ca^{2+} current I_{CaL}). Therefore, compared with baseline (all solid curves), with elevation of P_{up} to 20 mM/s (dashed curves), Ca^{2+} concentration in network SR (Fig. 2E) and junctional SR (Fig. 2I) both increased, leading to a faster rate of jSR refilling. Therefore, within a shorter time period that the higher jSR Ca^{2+} loads was attained, a secondary larger Ca^{2+} release during the DD period (red arrow in

the inset of Fig. 2G) drove a strong and fast increase of I_{NCX} (red arrow in Fig. 2B) to bring the membrane potential to threshold and produced an action potential with a shorter cycle time than the baseline.

When K_s was significantly reduced under the high P_{up} (all dotted curves), although accumulation of Ca^{2+} in jSR (Fig. 2I) and nSR (network SR, Fig. 2E) increased remarkably, Ca^{2+} release from the jSR (blue arrow in Fig. 2G) during the late DD decreased, resulting in smaller diastolic I_{NCX} than that during high P_{up} (about 35% decrease at the time indicated with the blue dashed lines in Fig. 2B), thereby increasing the time to bring the membrane potential to threshold and reducing the sinus rate. Of note, when I_{CaL} was activated, because of the high Ca^{2+} concentration in the jSR during CICR process, the third release (AP-induced) was strong in this situation, resulting in a higher peak of subspace Ca^{2+} (dotted curve in Fig. 2F) and I_{NCX} (dotted curve in Fig. 2B) than with the normal *K*s.

L-type Ca^{2+}current

I_{CaL} is one of the most important interactions between Ca^{2+} and M clocks because SR is reset and refueled by CICR process due to I_{CaL} activation. Fig. 3A showed effects of I_{CaL} on the electrical firing. To facilitate comparison, the baseline was plotted first with instant parameter changes (black bars) simulating various conditions explained with labels above the bars. Fig. 3Aa column corresponded to P_{up} 67% increase and *g*CaL 50% increase. As noted simultaneous increase P_{up} and *g*CaL resulted in fast sinus rate compared with baseline (15% rate increase). Large P_{up} led to the large I_{NCX} (arrow 1) and large Ca^{2+} release (arrow 2) during late DD. Increased *g*CaL further strengthened the CICR process, resulting in the large peak of Ca^{2+} release and I_{NCX} during fast firing of AP. However, if *g*CaL was reduced by 34% (Fig. 3Ab column), a notch (arrow 3) appeared in the phase 0 of the action potential with prolonged duration, implying delayed activation of I_{CaL}. Although Ca^{2+} release and I_{NCX} during late DD was still larger than that of the baseline due to the larger P_{up} (arrows 4 and 5), reduced *g*CaL made their peak value become small because of the suppressed CICR process. Further reduction of *g*CaL by 35% (Fig. 3Ac column) resulted in membrane oscillation (arrow 6) and spontaneous Ca^{2+} release (arrow 7) with sinus rhythm halt characterized with delayed afterdepolarization (DAD).

Fig. 3B explored effects of decreased I_{CaL} on AP firing under different values of P_{up}. If we define AP of Fig. 3Aa as rhythmic firing, Fig. 3Ab as firing with DAD, and Fig. 3Ac as no firing, Fig. 3B could be divided into three parts. Small *g*CaL led to failed firing even under the high P_{up} condition. Rhythmic firing existed only when the SR Ca^{2+} activity and I_{CaL} dynamically and properly interacted with each other. With decreasing P_{up}, large I_{CaL} was needed to sustain the rhythmic firing.

Hyperpolarization-activated “funny” current

I_f has long been considered as the most important ion channel involved in the rate regulation of cardiac pacemaker cells [3]. Fig. 4 showed change of sinus rate with gI_f (panel A), and a parametric analysis of sinus rate versus gI_f and P_{up} (panel B and C). Of note, complete blockade of gI_f made sinus rate fall to 2.86Hz, but without appearance of pause or abnormal firing. The rate modulation range was less than 0.3Hz when gI_f changed from 0.0nS/pF to two times of its baseline (0.30nS/pF). Even if gI_f was elevated to 0.6nS/pF the change of rate was less than 0.5Hz. But in panel C, blocking I_f and down-regulating P_{up} caused intermittent sinus pause. At the same low P_{up}, the persistent irregular firing (a) changed to transient irregular firing (b) and finally to rhythmic firing (c) by increasing gI_f. Also in B, increasing gI_f reduced the area of irregular firing at low P_{up}.

T-type Ca^{2+}current

Since T-type Ca^{2+} current (I_{CaT}) has a low activation threshold (~-60 mV), its activation was suggested as an additional mechanism contributing to the mid-late DD. Fig. 5 showed the role of I_{CaT} in sinus rate and rhythmic firing. As noted in the panel A, with decreasing of g_{CaT}, sinus rate gradually reduced. When g_{CaT} changed from 0.0nS/pF to two times of its baseline (0.3664nS/pF), the firing rate was smoothly regulated within the range of 2.67Hz to 3.33Hz. Four times of g_{CaT} resulted in a rate of 3.98Hz which was larger than the effect of I_f on sinus rate. Additionally, if the SR Ca^{2+} uptake rate was greatly inhibited as in panel B, a transient firing pause occurred after the suppression of P_{up}. But with I_{CaT} increased (from (a) to (c)), the time of sinus pause shortened and the firing recovered to the normal in the end.

Leading pacemaker site

We performed simulation on the developed fiber. In the first situation, when P_{up} increased linearly from 10 mM/s (superior) to 15 mM/s (inferior) along the strand, the leading pacemaker site located at the inferior region (Fig. 6Aa). In the second situation in which P_{up} increased exponentially, the inferior part was also the leading pacemaker site (Fig. 6Ab). In the third discontinuous situation, when P_{up} of the middle cells was 13mM/s in contrast to 12mM/s in other parts, the cells in the middle region exhibited the earliest electrical excitation and propagated towards the superior and inferior regions (Fig. 6Ba). Therefore, the above three cases consistently showed colocolization of the leading pacemaker site and the highest SERCA pump activity. To further test this relationship, on the bases of the conditions in Fig. 6Ba, we increased P_{up} of the superior cells by 30% and 15% for the middle and inferior cells. The results demonstrated that the leading pacemaker site shifted from the 15^{th} cell (red arrows) to the 30^{th} cell in the superior side (blue arrows in Fig. 6Bb) where the SR Ca^{2+}cycling was most active.

Additionally, relationship between the pacemaker site location, conduction velocity and the intercellular coupling conductance was assessed and summarized in Fig. 6Bc, where location of the earliest excitation was designated with the cell number. Leading pacemaker site and velocity both were plotted as a function of the coupling conductance between two neighboring cells, but with regards to the different y-axis. As noted, similar to the Fig. 6Ba and Fig. 6Bb, the leading pacemaker site always shifted from the 15^{th} cell in the middle (solid red circles) to the 30^{th} cell in the superior site (solid blue circles) if P_{up} of the superior cells became the maximum no matter what value the coupling conductance was. However, electrical conduction velocity from the superior to the inferior was greatly increased if the coupling conductance elevated from its baseline (7.5nS) to five times (37.5nS) (solid blue triangles).

Besides SR Ca^{2+} cycling, we found that I_{CaL} could also in some extent determine location of the earliest excitation. Based on the conditions in Fig. 6Bb, we suddenly decreased *g*CaL of the superior cells after the time notified with respective labels in Fig. 7. The action potential of the superior cell was shown in the upper panels while the lower panels displayed electrical propagations along the fiber. The leading pacemaker site was observed to shift from the superior (red arrows) towards the middle site (blue arrows) again. Comparing the gCaL effects, more suppressed *g*CaL caused more obvious shift of the leading pacemaker site.

Discussion

The present study focuses on the mechanistic investigation of recent experimental findings based on the latest mathematical model. Shortening of the jSR refilling time and increase of Ca^{2+} release from SR during DD were found to be responsible for the isoproterenol-induced sinus rate acceleration. In contrast with I_f and I_{CaT}, SR Ca^{2+} cycling was a major contributor to the broad sinus rate modulation. However, appearance of DAD-like firing at down-regulated

I_{CaL}, and stabilizing effect of I_f and I_{CaT} on sinus rhythm at suppressed SR Ca^{2+} cycling suggested the importance of membrane clock. In the simulated tissue, the leading pacemaker site was found to always colocalize with the site having the highest SR Ca^{2+} cycling, but I_{CaL} down-regulation also showed an obvious effect on the location.

Mechanisms of rate modulation and irregular firing

When the membrane clock was removed (all ion currents = 0), SR was shown to be a release-pump-delay oscillator, but unable to generate high-amplitude firing at higher rates[7]. Within the full system of two clocks, it was demonstrated that the interaction between the secondary releases of Ca^{2+} and I_{NCX} was responsible for producing rhythmic firing. Based on these findings, we investigated the combined effects of P_{up} and K_s on firing rate and the mechanisms to explain experimental observations, in which heart rate increased with elevated concentration of isoproterenol and decreased with infusion of ryanodine[18]. Fig. 2 suggested that increased SERCA pump activity by isoproterenol could markedly accelerate the rate of jSR refilling and increase the amount of Ca^{2+} release from SR during DD, thus shortening the time of I_{NCX} to threshold and thereby the cycle length. On the contrary, Ca^{2+} release inhibition by ryanodine would attenuate effects of isoproterenol and delay activation of I_{NCX}, resulting in sinus rate reduction. When P_{up}or $K_s$dramatically decreased, Ca^{2+} release from jSR was too small to activate $I_{NCX.}$ Then transient sinus pause occurred until accumulated Ca^{2+} was enough to trigger I_{NCX} and started a new action potential. In this case, the firings would most likely lose their intrinsic rhythm and became irregular as shown in Fig. 1.

We did the study under conditions of high P_{up} (higher than 12mM/s) and broad change of g_{CaL} (from 0 to 0.5nS/pF) to investigate their combined effects on automaticity. Area of rhythmic firing was found to extend with P_{up} elevation. Such results are in line with the finding in Ref.[7] and support the importance of Ca^{2+} clock. However, our results additionally suggested that even with higher P_{up}, lower contribution of I_{CaL} could lead to DAD-like firing and persistent sinus pause, implying a key role of I_{CaL} on rhythmic firing as well. Because I_{CaL} is mainly responsible for refilling the SR through Ca^{2+} influx and triggering CICR process, our results illustrated that the Ca^{2+} cycling could not be sustained when I_{CaL} was significantly down-regulated. Thus, after a spontaneous rhythmic Ca^{2+} release from the SR, depletion of Ca^{2+} in SR could cause sinus rhythm to completely stop after the DAD as observed in Fig. 3Ac. If down-regulation of I_{CaL} could be compensated by elevation of SERCA pump activity, which meant Ca^{2+} refueled into SR was just enough to maintain their cycling, then firing with DAD occurred as shown in Fig. 3Ab. In this case, because of decreased Ca^{2+} influx due to reduced I_{CaL}, increased SERCA pump would transport more Ca^{2+} into SR, thereby resulting in small Ca_{sub} concentration in submembrane space as shown in the trace of Ca_{sub} in Fig. 3Ab. This case was suggested to be a delicate balance between Ca^{2+} available for pumping and the speed of the SERCA pump, thus it only existed in a small area as shown in Fig. 3B. The above finding suggested importance of delicate corporation between SR Ca^{2+} cycling and I_{CaL} in keeping the system robustness.

In addition, we observed different effects of SR Ca^{2+} cycling and I_{CaL} on the action potential amplitude (APA). As observed in Fig. 1Ba and Fig. 1Bb, with increase of sinus rate, the maximum diastolic potential became more negative (from −57.5mV in Fig. 1Bb to −62.7mV in Fig. 1Ba), resulting in increase of APA. But 106.7% increase of the rate led to only 9.5% increase of APA. Therefore, the effect was only marginal. Nevertheless, as shown in Fig. 3, changes of I_{CaL} had obviously greater effects on APA. It might due to their different phases of function: SR Ca^{2+} cycling was mainly responsible for the spontaneous diastolic depolarization after the previous action potential to bring the membrane potential to threshold and activated I_{NCX}, while I_{CaL} was the primary current to generate the AP upstroke, thus should be the main factor to affect APA and overshoot.

Stabilization of the membrane currents on rhythmic firing

Activation of I_f and I_{CaT} were both suggested to be able to trigger a depolarization because of their low threshold [3]. In Ref.[7], the authors proved that inhibition of I_f resulted in rate reduction and the function of I_f in increasing the system robustness at low firing rates. On the other hand, our simulation in Fig. 4 demonstrated that compared with the rate modulation through SR Ca^{2+} cycling, I_f adjusted sinus rate within a narrow range (less than 0.3Hz) and without occurrence of firing pause at its blockade, suggesting a limited role of I_f in controlling pacemaker cell automaticity. Besides, as shown in Fig. 5 when g_{CaT} changed from 0.0nS/pF to 0.3664nS/pF, sinus rate was modulated within a range of 0.66Hz which was larger than that of $I_{f,}$ indicating the more important effect of I_{CaT} than I_f on rate adjustment. As noted in Fig. 4 and Fig. 5, similar to I_f, increase of I_{CaT} could stabilize the firing rhythm. But in contrast to I_f, complete elimination of I_{CaT} could not result in persistent sinus pause. Therefore, as far as keeping the rhythm stabilization was concerned, I_f was suggested to be more important than I_{CaT}. This might due to their different phases of activation, because I_f was mainly responsible for the earlier spontaneous DD while I_{CaT} was the primary current during the mid-late DD.

Effects of SR Ca^{2+} cycling and I_{CaL} on the leading pacemaker site

With the observation that the maximum LDCAE (late diastolic Ca_i elevation) slope always colocalized with the leading pacemaker site and that LDCAE could faithfully represent Ca^{2+} clock activity, the leading pacemaker site was proposed to be the site exhibiting the highest Ca^{2+} activity[18]. To test this proposal, we modified the distribution of P_{up} in various ways along the developed fiber. In either the linear, exponential or discontinuous situation, leading pacemaker site showed good consistency with the highest SR Ca^{2+}cycling.

In an optical mapping experiment, after isoproterenol infusion, the leading pacemaker site was found to shift to the superior SAN[18]. The SERCA2a/phospholamban molar ratio was reported lower in the superior SAN than the inferior SAN and right atrial tissue. The key regulator of SR Ca^{2+} uptake was phospholamban that inhibited SERCA2a in its dephosphorylated state, thereby superior site was supposed to have more phospholamban molecules available to regulate SERCA2a molecules and more robust Ca^{2+} uptake. We simulated this response by increasing P_{up} more in the superior than in other regions of the 1D model based on the third situation. The results in Fig. 6B confirmed the shift of the leading pacemaker site with increase of P_{up}. The site with the highest SERCA pump activity was characterized with the fastest and earliest spontaneous firing, driving the surrounding cells to fire and resulting in shift of the dominant pacemaker. Additionally, the results showed that the coupling conductance between neighboring cells had little effect on the location of the earliest excitation but velocity of the electrical propagation increased with the conductance elevation.

Besides, we observed the role of I_{CaL} in determining location of the earliest excitation. If I_{CaL} was suppressed as we did in Fig. 7, even with the superior cells showed the highest P_{up}, the leading pacemaker site still shifted to the site with less inhibited I_{CaL}. Note that in Fig. 7Aa and Fig. 7Ba, decreasing *g*CaL in the superior cells led to reduced amplitude of action potential, longer cycle length between the two neighboring action potentials and the appearance of DAD, thereby might suppress their dominant status in spontaneous activity. Consequently, in response to an intervention or diseased condition that suppresses the SAN spontaneous activity, the leading pacemaker is expected to shift to the site with the least suppressed intrinsic spontaneous activity, forming a hierarchical structure of pacemaker dominance.

Limitations

Because little is known about the heterogeneous distribution of the Ca^{2+} cycling in the SAN tissue, especially during β-adrenergic stimulation, we tested three cases and confirmed good

consistency between the leading pacemaker site and the highest SR Ca^{2+} activity, and the site shift with change of P_{up} as well. This tissue model provided us with an opportunity to exclusively investigate role of Ca^{2+} and I_{CaL} in determining the earliest pacemaker location. However, in reality, two-dimensional tissue would be more ideal and realistic in the study. Heterogeneities, such as cellular size, ionic currents and SR Ca^{2+}cycling among cells are neededfor further consideration.

The interaction of intracellular calcium dynamics and membrane current is a complicated process. We provided theoretical analysis of the SR Ca^{2+} cycling and effects of several main currents I_{CaL}, I_f and I_{CaT} on automaticity. However, other ionic channels, such as non-selective sustained current (I_{st}), was also suggested as additional mechanisms contributing to DD [19]. But due to its exhibition of many properties of I_{CaL} and $I_{NCX,}$ molecular origin and specific blockers of I_{st} have not been found yet, the identity of I_{st}remains unclear.

Supplementary Material

Refer to Web version on PubMed Central for supplementary material.

Acknowledgments

This study was supported in part by National Institutes of Health grants P01 HL78931, R01 HL78932, 71140, Chinese National Natural Science Foundation 30870659, 30971221 and Health Foundation of Shaanxi Province 08D23 (HZ), Medtronic-Zipes Endowments (PSC) and American Heart Association Established Investigator Award (SFL).

References

1. Chen PS, Joung B, Shinohara T, Das M, Chen ZH, Lin SF. The Initiation of the Heart Beat. Circ J 2010;74(2):221–225. [PubMed: 20019407]
2. Imai S, Saito F, Takase H, Enomoto M, Aoyama H, Yamaji S, Yokoyama K, Yagi H, Kushiro T, Hirayama A. Use of bepridil in combination with Ic antiarrhythmic agent in converting persistent atrial fibrillation to sinus rhythm. Circ J 2008;72(5):709–715. [PubMed: 18441448]
3. Baruscotti M, Bucchi A, DiFrancesco D. Physiology and pharmacology of the cardiac pacemaker ("funny") current. Pharmacology & Therapeutics 2005;107(1):59–79. [PubMed: 15963351]
4. Brown HF, DiFrancesco D, Noble SJ. How does adrenaline accelerate the heart? Nature 1979;280:235–236. [PubMed: 450140]
5. Maltsev VA, Vinogradova TM, Lakatta EG. The emergence of a general theory of the initiation and strength of the heartbeat. J Pharmacol Sci 2006;100(5):338–369. [PubMed: 16799255]
6. Vinogradova TM, Lyashkov AE, Zhu WZ, Ruknudin AM, Sirenko S, Yang DM, Deo S, Barlow M, Johnson S, Caffrey JL, Zhou YY, Xiao RP, Cheng HP, Stern MD, Maltsev VA, Lakatta EG. High basal protein kinase A-dependent phosphorylation drives rhythmic internal Ca2+ store oscillations and spontaneous beating of cardiac pacemaker cells. Circulation Research 2006;98(4):505–514. [PubMed: 16424365]
7. Maltsev VA, Lakatta EG. Synergism of coupled subsarcolemmal Ca2+ clocks and sarcolemmal voltage clocks confers robust and flexible pacemaker function in a novel pacemaker cell model. Am J Physiol Heart Circ Physiol 2009;296(3):H594–615. [PubMed: 19136600]
8. Yano M. Ryanodine receptor as a new therapeutic target of heart failure and lethal arrhythmia. Circ J 2008;72(4):509–514. [PubMed: 18362417]
9. Bleeker WK, Mackaay AJ, Masson-Pevet M, Bouman LN, Becker AE. Functional and morphological organization of the rabbit sinus node. Circ Res 1980;46(1):11–22. [PubMed: 7349910]
10. Dobrzynski H, Li J, Tellez J, Greener ID, Nikolski VP, Wright SE, Parson SH, Jones SA, Lancaster MK, Yamamoto M, Honjo H, Takagishi Y, Kodama I, Efimov IR, Billeter R, Boyett MR. Computer three-dimensional reconstruction of the sinoatrial node. Circulation 2005;111(7):846–854. [PubMed: 15699261]

11. Zhang H, Holden AV, Boyett MR. Gradient model versus mosaic model of the sinoatrial node. Circulation 2001;103(4):584–588. [PubMed: 11157726]
12. Garny A, Kohl P, Hunter PJ, Boyett MR, Noble D. One-dimensional rabbit sinoatrial node models: benefits and limitations. J Cardiovasc Electrophysiol 2003;14(10 Suppl):S121–132. [PubMed: 14760914]
13. Shibata N, Inada S, Mitsui K, Honjo H, Yamamoto M, Niwa R, Boyett MR, Kodama I. Pacemaker shift in the rabbit sinoatrial node in response to vagal nerve stimulation. Exp Physiol 2001;86(2): 177–184. [PubMed: 11429632]
14. Dobrzynski H, Boyett MR, Anderson RH. New insights into pacemaker activity - Promoting understanding of sick sinus syndrome. Circulation 2007;115(14):1921–1932. [PubMed: 17420362]
15. Opthof T. Embryological development of pacemaker hierarchy and membrane currents related to the function of the adult sinus node: implications for autonomic modulation of biopacemakers. Medical & Biological Engineering & Computing 2007;45(2):119–132. [PubMed: 17203321]
16. Verheule S, van Kempen MJ, Postma S, Rook MB, Jongsma HJ. Gap junctions in the rabbit sinoatrial node. Am J Physiol Heart Circ Physiol 2001;280(5):H2103–2115. [PubMed: 11299212]
17. Eisner DA, Kashimura T, Venetucci LA, Trafford AW. From the ryanodine receptor to cardiac arrhythmias. Circ J 2009;73(9):1561–1567. [PubMed: 19667488]
18. Joung B, Tang L, Maruyama M, Han S, Chen Z, Stucky M, Jones LR, Fishbein MC, Weiss JN, Chen PS, Lin SF. Intracellular calcium dynamics and acceleration of sinus rhythm by beta-adrenergic stimulation. Circulation 2009;119(6):788–U751. [PubMed: 19188501]
19. Maltsev VA, Lakatta EG. Dynamic interactions of an intracellular Ca2+ clock and membrane ion channel clock underlie robust initiation and regulation of cardiac pacemaker function. Cardiovasc Res 2008;77(2):274–284. [PubMed: 18006441]

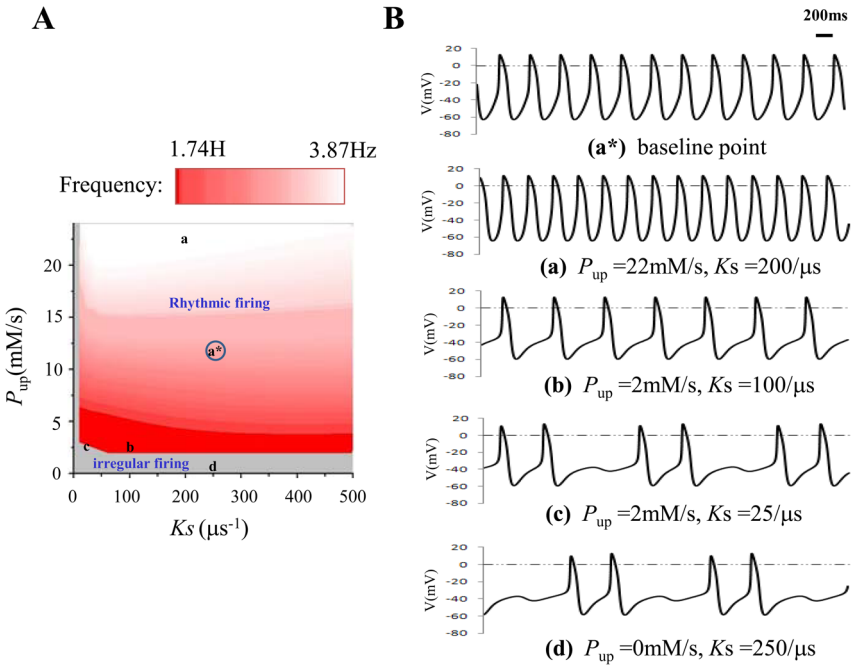

Figure 1.

Effects of SR Ca^{2+} cycling on sinus rate. Panel A: P_{up} (Ca^{2+} pump rate) changed from 0.0mM/s to 24.0mM/s with the step size of 1.0mM/s. K_s (SR Ca^{2+} release rate) changed from 0.0/μs to 500/μs with the step size of 10/μs. Grey area represented the irregular firing while red area corresponded to the rhythmic firing. Panel B: some specific action potentials positioned in Panel A. a* was the baseline point (P_{up} =12mM/s, Ks =250/μs). a and b were two points which showed regular firings but with different sinus rates. c and d displayed two sites showing irregular firings.

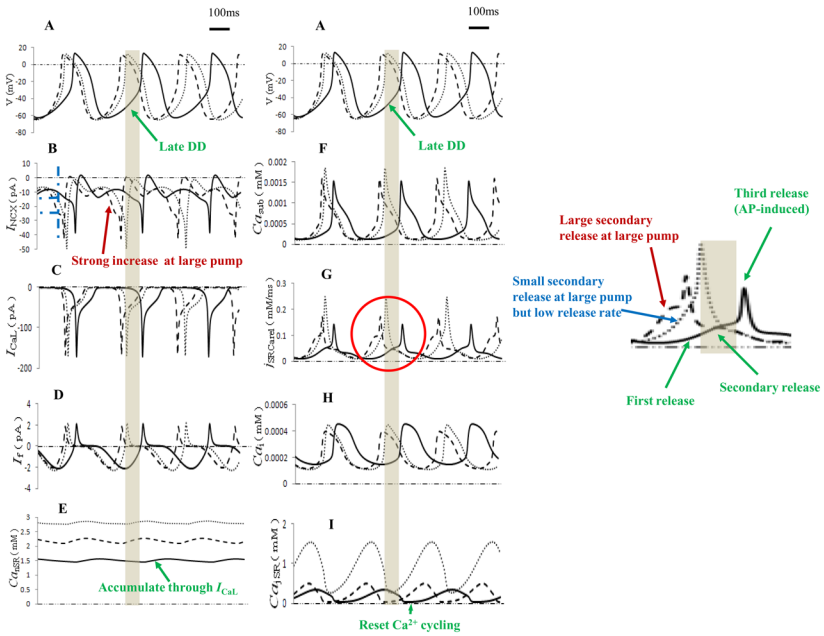

Figure 2.

Simulation traces of the primary dynamic interactions of the M clock and Ca^{2+} clock during spontaneous production of action potential. Action potentials, major ionic currents and Ca^{2+} behaviors in different compartments were shown. Solid curves denoted the baseline (P_{up} =12mM/s, K_s =250/μs). Dashed curves were under the high SERCA pump rate (P_{up} =20mM/s, K_s =250/μs) while dotted curves corresponded to the high SERCA pump but low Ca^{2+} release rate (P_{up} =20mM/s, K_s =12.5/μs). Grey bars indicated the period of late DD under the baseline conditions. The jSRCarel curves inside the red circle were enlarged at the right side.

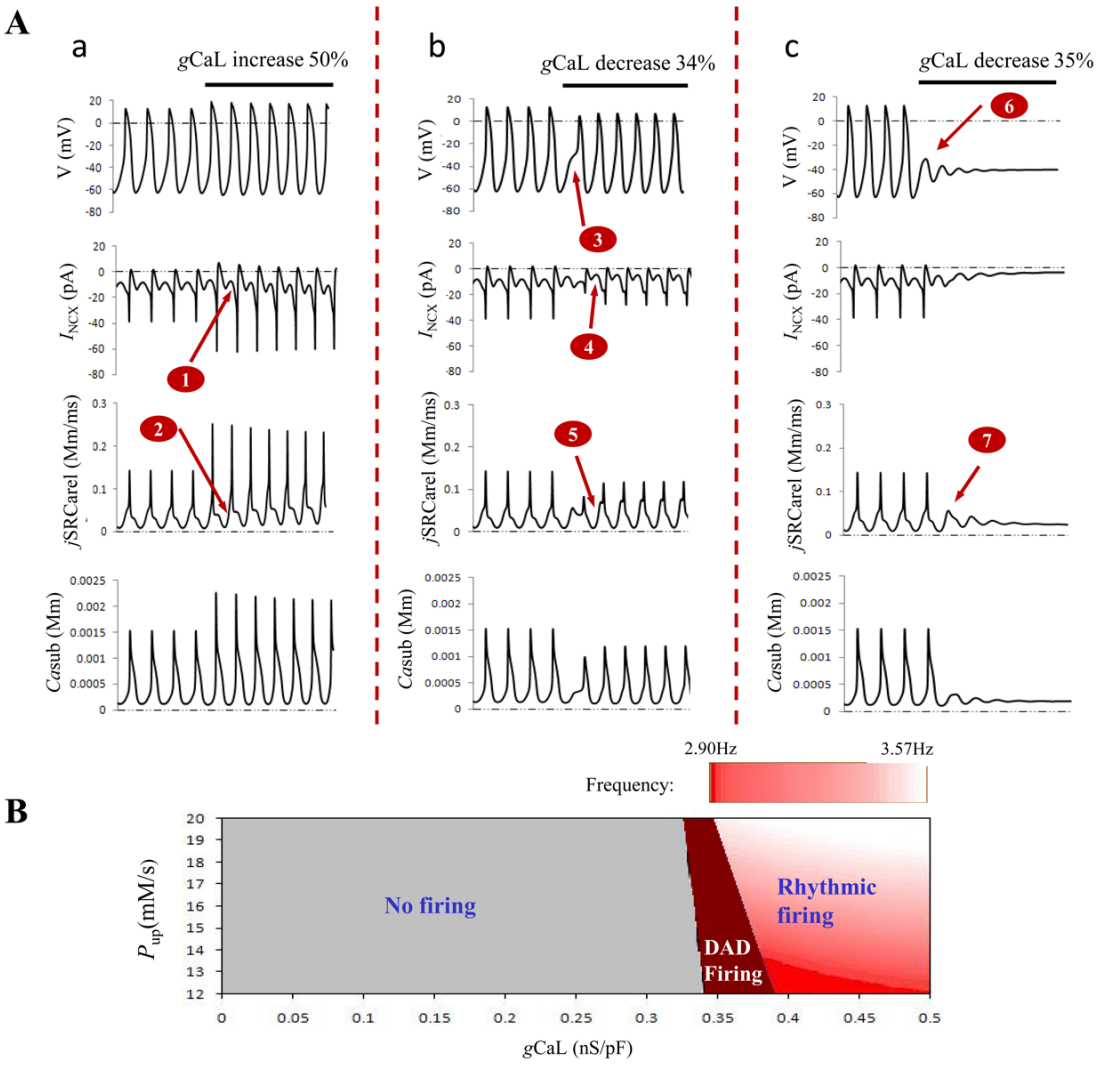

Figure 3.

Effects of I_{CaL} on rhythmic AP firing. Panel A: Action potentials, major ionic and Ca^{2+} changes during large P_{up} (67% higher than baseline) and large *g*CaL (50% increase) (a), or large P_{up} and small *g*CaL (34% decrease in (b) and 35% decrease in (c)). Panel B: exploration of AP firing with variations of P_{up} and *g*CaL at the same time. The steps for P_{up} and *g*CaL were 1.0mM/s and 0.001nS/pF, respectively.

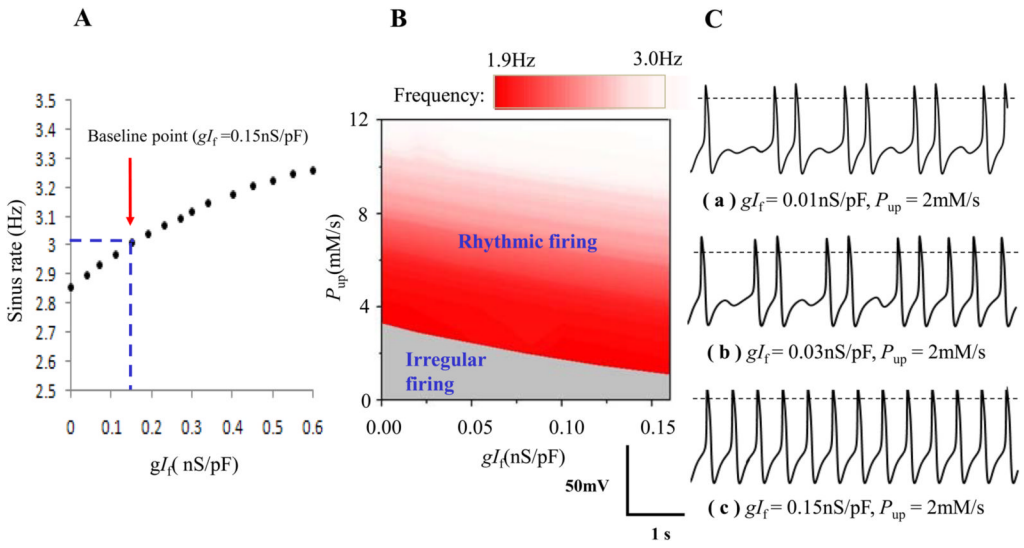

Figure 4.

Role of I_f in the rhythmic firing of the whole system. A: sinus rate modulation by I_f. B: analysis of P_{up} and gI_f. The step size was 0.01nS/pF for gI_f and 0.2mM/s for P_{up}. Action potentials of the three specific points within the panel A were depicted in panel C.

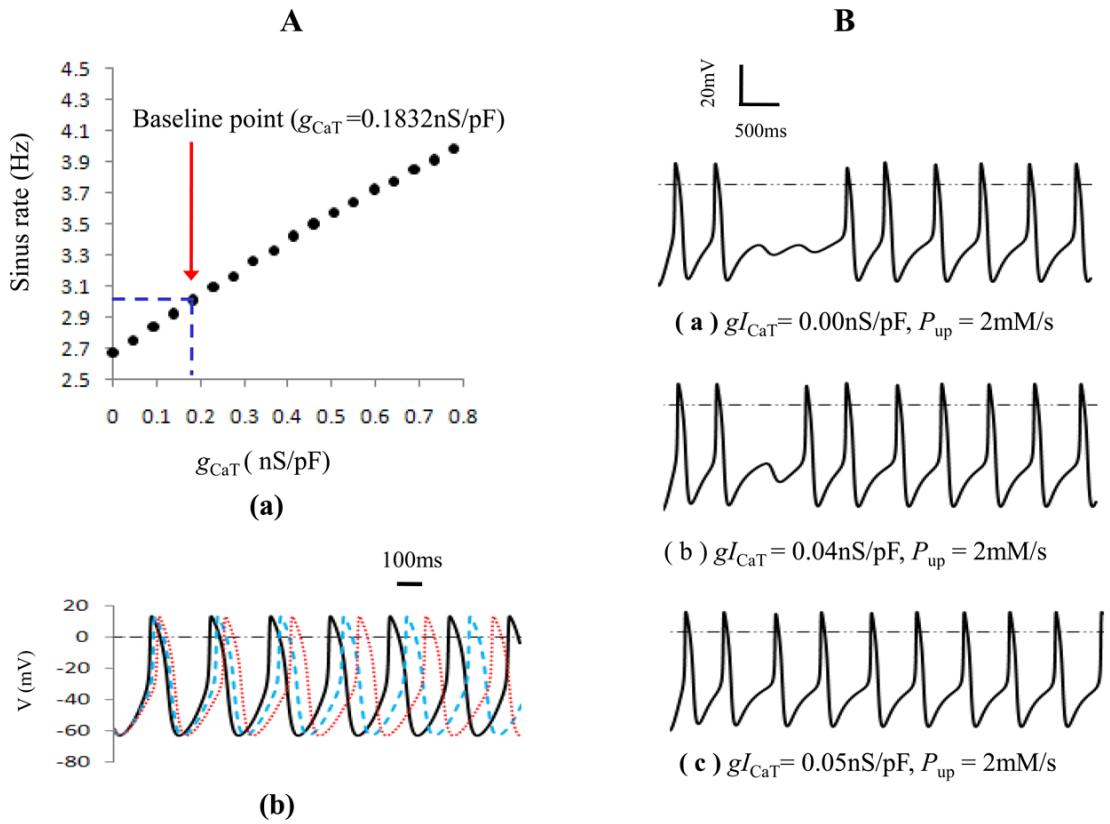

Figure 5.

Role of I_{CaT} in sinus rate and rhythmic firing. Panel A: (a) relationship between g_{CaT} and sinus rate. (b) Action potentials at g_{CaT} 0.1832nS/pF (solid lines), 0.09nS/pF (dashed lines) and 0.00 nS/pF (dotted lines), respectively. Panel B: Role of I_{CaT} at the low Ca^{2+} pump rate.

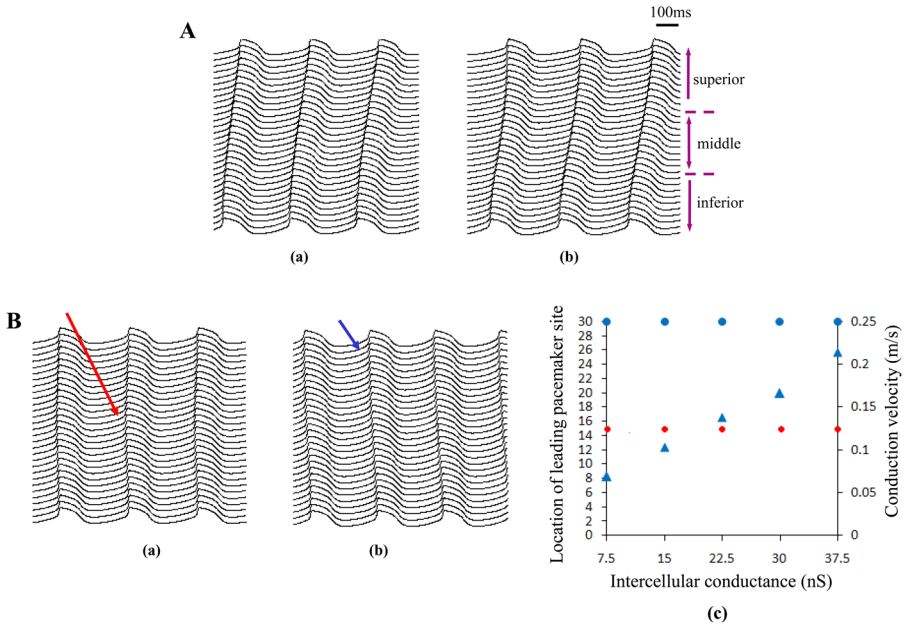

Figure 6.

Role of Ca^{2+}clock in determining the leading pacemaker site in a sin us node fiber. Panel A: electrical propagation when Ca^{2+} uptake rate (P_{up}) was smoothly changed in a linear (a) or exponential (b) way along the strand from 10mM/s (superior) to 15mM/s (inferior). Along the strand the upper 10 cells was defined as the superior site, the lower 10 cells was defined as the inferior site as denoted. Panel B: leading pacemaker site shifted from the middle (red arrow in a,) to the superior (blue arrow in b,) when P_{up} of the superior cells increased 30% while other cells only had 15% increase. (c) showed relationship of the intercellular conductance with the location of leading pacemaker site and conduction velocity. Similar to the (a) and (b), the earliest excitation always shifted from the 15^{th} cell in the middle (solid red circles) to the 30^{th} cell in the superior site (solid blue circles) if P_{up} of the superior cells became the maximum no matter what value the coupling conductance was. But electrical conduction velocity from the superior to the inferior was greatly increased (solid blue triangles) if the coupling conductance elevated from its baseline (7.5nS) to five times (37.5nS).

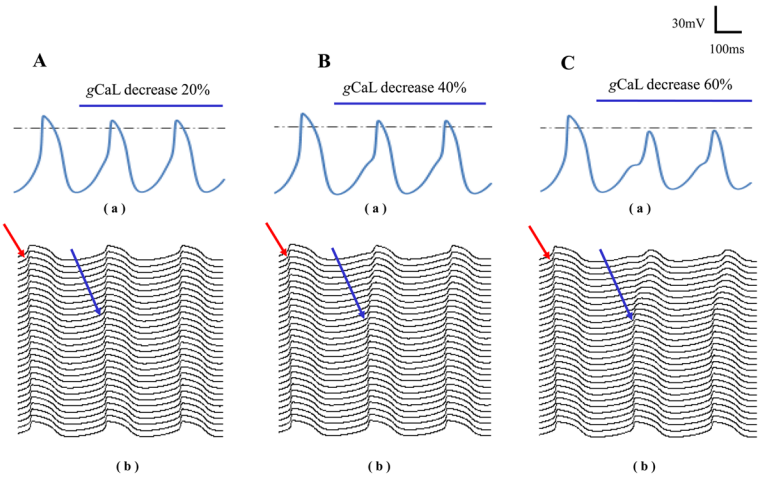

Figure 7.

Effects of I_{CaL} on the leading pacemaker site. *g*CaL of the superior cells was changed after the time indicated with respective labels in each panel. Their action potentials were shown in (a) while (b) displayed electrical propagations along the fiber. Before changing *g*CaL, action potential propagated from the superior to the inferior as indicated by the red arrows. After decreasing *g*CaL, leading pacemaker site started to shift towards the middle site indicated by the blue arrows.